

Numerical simulation of non-isothermal flow in oil reservoirs using a two-equation model

Juan Diego dos Santos Heringer*, João Gabriel de Souza Debossam, Grazione de Souza and Helio Pedro Amaral Souto

Polytechnic Institute, Rio de Janeiro State University, Nova Friburgo, Brazil

(Received September 28, 2018, Revised December 26, 2018, Accepted January 31, 2019)

Abstract. This work aims to simulate three-dimensional heavy oil flow in a reservoir with heater-wells. Mass, momentum and energy balances, as well as correlations for rock and fluid properties, are used to obtain non-linear partial differential equations for the fluid pressure and temperature, and for the rock temperature. Heat transfer is simulated using a two-equation model that is more appropriate when fluid and rock have very different thermal properties, and we also perform comparisons between one- and two-equation models. The governing equations are discretized using the Finite Volume Method. For the numerical solution, we apply a linearization and an operator splitting. As a consequence, three algebraic subsystems of linearized equations are solved using the Conjugate Gradient Method. The results obtained show the suitability of the numerical method and the technical feasibility of heating the reservoir with static equipment.

Keywords: finite volume method; heating techniques; non-isothermal flow; oil reservoir; operator splitting; reservoir simulation

1. Introduction

Enhanced oil recovery (EOR) or tertiary recovery is commonly applied to extract an extra amount of oil from the reservoir, after primary (oil extracted by natural drive mechanism) and secondary (immiscible fluid injection) recovery. EOR techniques include chemical, miscible displacement, biological and thermal methods which aim to enhance hydrocarbons recovery by changing the fluid properties. For example, we have heavy oil extraction using thermal methods to reduce oil viscosity (Aouizerate, Durlofsky and Samier 2011). According to Eduardo (2010), the non-isothermal flow in porous media has attracted the interest of many engineers and scientists since the rock and fluid properties depend on pressure and temperature in a realistic process.

Nowadays there are several thermal methods used to heat hydrocarbons reservoir, for example, heated water injection, in-situ combustion, and steam injection. Ezeuko and Gates (2018) investigated heavy oil recovery in fractured reservoirs (Nikolic, Ibrahimbegovic and Miscovic 2016, Hadzalic,

*Corresponding author, E-mail: jheringer@iprj.uerj.br

Ibrahimbegovic and Dolarevic 2018, Hadzalic, Ibrahimbegovic and Nikolic 2018) using steam injection and analyzed thermal recovery benefits, for example. There are also static heaters, which were studied by Hazra (2014) considering different methodologies used by oil companies in hydrocarbon recovery from oil shale. The static heaters category includes different mechanical structures (such as an antenna), based on microwave or electricity, for example. In recent years, research and development related to static heaters have increased, and they have been used to improve heavy oil displacement without fluid injection. The heaters add thermal energy to a specific region of the reservoir to heat both rock and fluid, as shown in Fig. 1.

Physical-mathematical modeling for non-isothermal flow must take into account mass, momentum and energy balances and also, boundary and initial conditions. In the so-called one-equation models (Rousset, Huang and Durlofsky 2014), a single temperature (fluid and rock average temperatures are supposed to be equal) or an average temperature are introduced to represent the porous media temperature. As described by Moyné *et al.* (2000), when we do not assume the local thermal equilibrium, a volume average temperature is defined as the weighted average of the fluid and rock temperatures (from the definition of enthalpy). Therefore, both rock and oil have distinct temperatures, and a source term in the macroscopic equations takes into account the heat transfer between the fluid and solid phases (Lampe 2013, Moyné and Amaral Souto 2014a, b). Both models have been used to simulate non-isothermal flow in porous media. The accuracy of each model depends on the relationship between the rock and fluid thermal properties of the fluid and the rock phases. In general, the two-equation model (although more complex) is more comprehensive than the one-equation model (easier to implement). Therefore, one of the objectives of this work is the determination of the pertinence of the use of both models in the considered context.

This work is concerned with the numerical simulation of non-isothermal three-dimensional heavy oil flow in a reservoir containing static heaters. Mass, momentum and energy balances, as well as correlations for rock and fluid properties (as a function of pressure and temperature), are used to obtain the governing non-linear partial differential equations, considering a two-equation model to compute the heat transfer in the reservoir. The governing equations are discretized using the Finite Volume Method (Moukalled, Mangani and Darwish 2016), and the system of algebraic equations are solved using the Conjugate Gradient Method along with a Picard linearization procedure (Nick *et al.* 2013) and an operator splitting technique (Dyrdahl 2014).

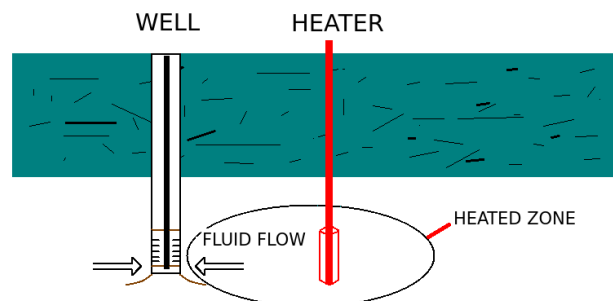


Fig. 1 Heating process using static heaters

2. Balance equations in porous media flow

Based on mass, momentum, and energy conservation principles, we can derive macroscopic equations that model fluid flow and energy transfer in porous media (Lampe 2013).

2.1 Mass balance and momentum equation

Mass balance equation is represented by (Ertekin, Abou-Kassem and King 2001)

$$\frac{\partial}{\partial t} \left(\frac{\phi}{B} \right) + \nabla \cdot \left(\frac{\mathbf{v}}{B} \right) - \frac{q_{sc}}{V_b} = 0, \quad (1)$$

where ϕ and $B = \rho_f / \rho_{sc}$ are the porosity and the formation-volume-factor (FVF), respectively, q_{sc} is a source term in standard conditions (sc), V_b is the bulk volume, and the apparent velocity is represented by \mathbf{v} and it is given by the Darcy's law (Ertekin, Abou-Kassem and King 2001)

$$\mathbf{v} = -\frac{\mathbf{k}}{\mu} (\nabla p - \rho_f g \nabla D), \quad (2)$$

where \mathbf{k} is the porous media absolute permeability tensor, μ is the fluid viscosity, p is the pressure, ρ_f is the fluid density, g is the magnitude of gravity and D represents the depth. The fluid viscosity depends on temperature and is calculated by (Rousset, Huang and Durlofsky 2014)

$$\mu = a \exp \left(\frac{b}{T - T_{ref,\mu}} \right) \quad (3)$$

where a , b and $T_{ref,\mu}$ must be provided.

Considering that the porosity and the formation-volume-factor are functions of pressure and temperature (Rousset, Huang and Durlofsky 2014)

$$\phi = \phi^0 [1 + c_r (p - p^0) - c_{rT} (T_r - T_r^0)], \quad B = \frac{B^0}{1 + c_f (p - p^0) - c_{fT} (T_f - T_f^0)}, \quad (4)$$

where the superscript 0 represents the reference value, c_r and c_f are the compressibilities for the rock and the oil, T_r and T_f are the temperatures of the rock and the fluid, and c_{rT} and c_{fT} are the coefficients of thermal expansion for the rock and the fluid respectively, it is possible to obtain

$$\frac{\partial}{\partial t} \left(\frac{\phi}{B} \right) = \frac{\partial p}{\partial t} \left[\frac{1}{B} \frac{\partial \phi}{\partial p} + \phi \frac{\partial}{\partial p} \left(\frac{1}{B} \right) \right] + \frac{\partial T_r}{\partial t} \left(\frac{1}{B} \frac{\partial \phi}{\partial T_r} \right) + \frac{\partial T_f}{\partial t} \left[\phi \frac{\partial}{\partial T_f} \left(\frac{1}{B} \right) \right]. \quad (5)$$

Taking the partial derivative of ϕ with respect to p and T_r , and of B with respect to p and T_f ,

$$\frac{\partial}{\partial t} \left(\frac{\phi}{B} \right) = \left(\frac{\phi^0 c_r}{B} + \frac{\phi c_f}{B^0} \right) \frac{\partial p}{\partial t} - \left(\frac{\phi^0 c_{rT}}{B} \right) \frac{\partial T_r}{\partial t} - \left(\frac{\phi c_{fT}}{B^0} \right) \frac{\partial T_f}{\partial t}. \quad (6)$$

Replacing Eqs. (6) and (2) into Eq. (1) we obtain

$$\Gamma_p \frac{\partial p}{\partial t} - \Gamma_{T_r} \frac{\partial T_r}{\partial t} - \Gamma_{T_f} \frac{\partial T_f}{\partial t} - \nabla \cdot \left[\frac{\mathbf{k}}{\mu B} (\nabla p - \rho_f g \nabla D) \right] - \frac{q_{sc}}{V_b} = 0 \quad (7)$$

where

$$\Gamma_p = \frac{\phi c_f}{B^0} + \frac{\phi^0 c_r}{B}, \quad \Gamma_{T_r} = \frac{\phi^0 c_{rT}}{B}, \quad \Gamma_{T_f} = \frac{\phi c_{fT}}{B^0}. \quad (8)$$

2.2 Energy balance

In this work, we do not assume the local thermal equilibrium hypothesis. In other words, the average temperatures of rock and fluid are not equal, and the heat transfer between both fluid and rock phases is modeled by macroscopic source terms (Moyne and Amaral Souto 2014a, b, Rousset, Huang and Durlofsky 2014). Hence, the rock energy balance equation is given by (based on Lampe (2013) and Moyne and Amaral Souto (2014a))

$$\frac{\partial}{\partial t}[(1 - \phi)\rho_r c_{pr} T_r] - \nabla \cdot [(1 - \phi)\mathbf{K}_r \nabla T_r] + AH(T_r - T_f) - (1 - \phi)\frac{q_H}{V_b} = 0 \quad (9)$$

while for the fluid we have (based on Lampe (2013) and Moyne and Amaral Souto (2014a))

$$\frac{\partial}{\partial t}(\phi\rho_f c_{pf} T_f) - \nabla \cdot (\phi\mathbf{K}_f \nabla T_f) + \nabla \cdot (\rho_f h_f \mathbf{v}) - AH(T_r - T_f) - \phi\frac{q_H}{V_b} - \frac{\rho_f h_f q_{sc}}{V_b} = 0, \quad (10)$$

where ρ_r is the rock density, c_{pf} and c_{pr} are the specific heats of rock and fluid, respectively, $h_f = c_{pf} T_f$ approximate the fluid enthalpy (Rousset, Huang and Durlofsky 2014), and \mathbf{K}_f and \mathbf{K}_r represent the effective thermal dispersion tensors. A is the superficial specific area of the fluid-solid interface, H is the effective heat transfer coefficient, q_H/V_b represents the increase or decrease of heat on the reservoir due to the heaters, and $\rho_f h_f q_{sc}/V_b$ represents the gain or loss of energy by injection or extraction of fluid into or from the reservoir.

We only consider here the contribution due to the thermal conductivity, and we neglect tortuosity and hydrodynamic dispersion contributions (Moyne *et al.* 2000). However, this procedure is commonly used (Lampe 2013). Therefore, we assume that $\mathbf{K}_f = \kappa_f \mathbf{I}$ and $\mathbf{K}_r = \kappa_r \mathbf{I}$, where κ_f and κ_r are the thermal conductivities of fluid and rock, respectively. For the two-equation model, the intrinsic volume average temperatures are then determined by directly solving the macroscopic temperature equations for each phase (Moyne and Amaral Souto 2014a).

2.3 Initial and boundary conditions

Eqs. (7), (9) and (10), which describe the single-phase non-isothermal fluid flow in porous media is not complete unless we specify initial and boundary conditions.

As initial conditions, we impose, in spite of the geothermal gradient (0.03 to 0.04 K/m approximately), a constant temperature value for the oil and rock everywhere in the reservoir. For the oil pressure, we impose a pre-established value at a given position (depth), and the other values are calculated according to the hydrostatic gradient.

We also use no flow conditions (Neumann boundary condition) at the reservoir boundaries. We apply these boundary conditions for both mass and heat flux, and they indicate that there is no mass flow and energy transfer across the boundaries of the reservoir.

3. Numerical solution methodology

The Finite Volume Method (FVM) is a numerical method for solving partial differential equations based on a volume integral formulation with a partitioning set of volumes (elements or cells) to discretized the domain (Moukalled, Mangani and Darwish 2016). The discretized partial differential equations give rise to a system of coupled non-linear algebraic equations.

3.1 Spatial and time discretizations

This method ensures integral conservation of mass, momentum, and energy over any group of control volumes and over the whole solution domain. The method consists of three steps. The first accounts for partitioning the domain into discrete control volumes using a computational grid. For each finite volume created, there is a corresponding associated balance equation. We introduce now the system of notation adopted here for the finite volume, with a central node point, shown in Fig. 2. The finite volume interfaces are represented by: $(i - 1/2, j, k) = w$, $(i + 1/2, j, k) = e$, $(i, j - 1/2, k) = n$, $(i, j + 1/2, k) = s$, $(i, j, k - 1/2) = b$ and $(i, j, k + 1/2) = a$, where w , e , n , s , b and a stand for *west*, *east*, *north*, *south*, *below* and *above* respectively. The central node is designated as $P(i, j, k)$, and the neighbor nodes are represented by $(i - 1, j, k) = W$, $(i + 1, j, k) = E$, $(i, j - 1, k) = N$, $(i, j + 1, k) = S$, $(i, j, k - 1) = A$ and $(i, j, k + 1) = B$.

The second step is the discretization of the governing equations, obtained from the integration of the partial differential equations, in time and space, over each finite volume to yield discretized equations for each nodal point P , on which the unknowns are calculated. As a result of the integration, some properties and gradients need to be evaluated at finite volume interfaces. A central-difference scheme is an accurate way of calculating the derivatives, and the properties are approximated using harmonic and weighted averages (Ertekin, Abou-Kassem and King 2001). After the spatial integration, we perform the time integration considering a conservative expansion of the time derivatives as discussed by Ertekin, Abou-Kassem and King (2001).

The resultant discretized equation for the pressure is

$$\Phi_x \Big|_{i+1/2,j,k}^{n+1} (p_{i+1,j,k} - p_{i,j,k})^{n+1} - \Phi_x \Big|_{i-1/2,j,k}^{n+1} (p_{i,j,k} - p_{i-1,j,k})^{n+1}$$

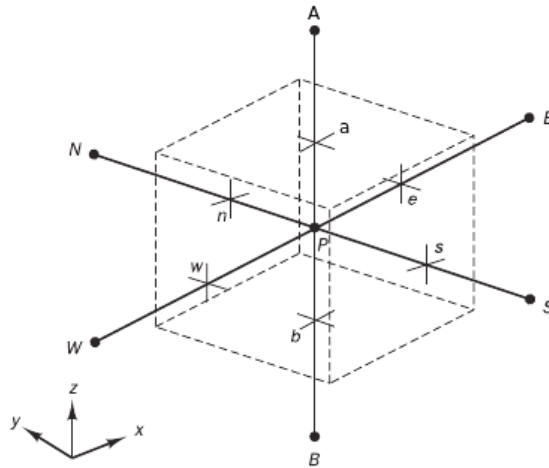


Fig. 2 A finite volume surrounding a central node point on a mesh

$$\begin{aligned}
& + \Phi_y \Big|_{i,j+1/2,k}^{n+1} (p_{i,j+1,k} - p_{i,j,k})^{n+1} - \Phi_y \Big|_{i,j-1/2,k}^{n+1} (p_{i,j,k} - p_{i,j-1,k})^{n+1} \\
& + \Phi_z \Big|_{i,j,k+1/2}^{n+1} (p_{i,j,k+1} - p_{i,j,k})^{n+1} - \Phi_z \Big|_{i,j,k-1/2}^{n+1} (p_{i,j,k} - p_{i,j,k-1})^{n+1} \\
& - \frac{(\Gamma_p)_{i,j,k}}{\Delta t} (p_{i,j,k}^{n+1} - p_{i,j,k}^n) + \frac{(\Gamma_{T_f})_{i,j,k}}{\Delta t} (T_{f,i,j,k}^{n+1} - T_{f,i,j,k}^n) + \frac{(\Gamma_{T_r})_{i,j,k}}{\Delta t} (T_{r,i,j,k}^{n+1} - T_{r,i,j,k}^n) \\
& + (\Omega_z)_{i,j,k+1/2}^{n+1} (D_{i,j,k+1} - D_{i,j,k}) - (\Omega_z)_{i,j,k-1/2}^{n+1} (D_{i,j,k} - D_{i,j,k+1}) + q_{sc,i,j,k}^{n+1} = 0 \quad (11)
\end{aligned}$$

where the transmissibility terms (for x -direction) are defined as

$$(\Phi_x) \Big|_e = \left(\frac{A_x k_x}{\mu B \Delta x} \right)_e, \quad (\Phi_x) \Big|_w = \left(\frac{A_x k_x}{\mu B \Delta x} \right)_w, \quad (12)$$

while for the hydrostatic terms we have

$$(\Omega_z) \Big|_a = \left(\frac{A_z k_z \rho_f g}{\mu B \Delta z} \right)_a, \quad (\Omega_z) \Big|_b = \left(\frac{A_z k_z \rho_f g}{\mu B \Delta z} \right)_b, \quad (13)$$

and the term A represents the finite volume interface areas, in x -, y - and z - directions: $A_x = \Delta y \Delta z$, $A_y = \Delta x \Delta z$ and $A_z = \Delta x \Delta y$.

On the other hand, from Eq. (9) we obtain

$$\begin{aligned}
& (1 - \phi) (\Lambda_r)_x \Big|_{i+1/2,j,k}^{n+1} (T_{r,i+1,j,k} - T_{r,i,j,k})^{n+1} - (\Lambda_r)_x \Big|_{i-1/2,j,k} (T_{r,i,j,k} - T_{r,i-1,j,k})^{n+1} \\
& + (1 - \phi) (\Lambda_r)_y \Big|_{i,j+1/2,k}^{n+1} (T_{r,i,j+1,k} - T_{r,i,j,k})^{n+1} - (\Lambda_r)_y \Big|_{i,j-1/2,k} (T_{r,i,j,k} - T_{r,i,j-1,k})^{n+1} \\
& + (1 - \phi) (\Lambda_r)_z \Big|_{i,j,k+1/2}^{n+1} (T_{r,i,j,k+1} - T_{r,i,j,k})^{n+1} - (\Lambda_r)_z \Big|_{i,j,k-1/2} (T_{r,i,j,k} - T_{r,i,j,k-1})^{n+1} \\
& - V_b \left[\frac{(1 - \phi) \rho c_{cp}}{\Delta t} \right]_{i,j,k}^{n+1} (T_{r,i,j,k}^{n+1} - T_{r,i,j,k}^n) + V_{b,i,j,k} A H (T_r - T_f)_{i,j,k}^{n+1} + (1 - \phi) q_H \Big|_{i,j,k}^{n+1} = 0, \quad (14)
\end{aligned}$$

and, finally, for Eq. (10),

$$\begin{aligned}
& \phi (\Lambda_f)_x \Big|_{i+1/2,j,k}^{n+1} (T_{f,i+1,j,k} - T_{f,i,j,k})^{n+1} - (\Lambda_f)_x \Big|_{i-1/2,j,k} (T_{f,i,j,k} - T_{f,i-1,j,k})^{n+1} \\
& + \phi (\Lambda_f)_y \Big|_{i,j+1/2,k}^{n+1} (T_{f,i,j+1,k} - T_{f,i,j,k})^{n+1} - (\Lambda_f)_y \Big|_{i,j-1/2,k} (T_{f,i,j,k} - T_{f,i,j-1,k})^{n+1}
\end{aligned}$$

$$\begin{aligned}
 & +\phi(\Lambda_f)_z \Big|_{i,j,k+1/2}^{n+1} (T_{f,i,j,k+1} - T_{f,i,j,k})^{n+1} - (\Lambda_f)_z \Big|_{i,j,k-1/2} (T_{f,i,j,k} - T_{f,i,j,k-1})^{n+1} \\
 & -(\Psi_z)_{i,j,k+1/2}^{n+1} (D_{i,j,k+1} - D_{i,j,k}) + (\Psi_z)_{i,j,k-1/2}^{n+1} (D_{i,j,k} - D_{i,j,k+1}) - \bar{\Theta}_{x,y,z} \\
 & -V_b \left(\frac{\phi \rho c_{cp}}{\Delta t} \right)_{i,j,k}^{n+1} (T_{f,i,j,k}^{n+1} - T_{f,i,j,k}^n) + (\rho_f h_f q_{sc})_{i,j,k}^{n+1} - V_{b,i,j,k} A H (T_r - T_f)_{i,j,k}^{n+1} + \phi q_H \Big|_{i,j,k}^{n+1} = 0
 \end{aligned} \tag{15}$$

where

$$\begin{aligned}
 \bar{\Theta}_{x,y,z} &= (h\Phi_x)_{i-1/2,j,k}^{n+1} (p_{i,j,k} - p_{i-1,j,k})^{n+1} - (h\Phi_x)_{i+1/2,j,k}^{n+1} (p_{i+1,j,k} - p_{i,j,k})^{n+1} \\
 &+ (h\Phi_y)_{i,j-1/2,k}^{n+1} (p_{i,j,k} - p_{i,j-1,k})^{n+1} - (h\Phi_y)_{i,j+1/2,k}^{n+1} (p_{i,j+1,k} - p_{i,j,k})^{n+1} \\
 &+ (h\Phi_z)_{i,j,k-1/2}^{n+1} (p_{i,j,k} - p_{i,j,k-1})^{n+1} - (h\Phi_z)_{i,j,k+1/2}^{n+1} (p_{i,j,k+1} - p_{i,j,k})^{n+1},
 \end{aligned} \tag{16}$$

and also for the energy equations, we introduce

$$(\Lambda_\alpha) \Big|_w = \left(\frac{A_x(\kappa_\alpha)x}{\Delta x} \right)_w, \quad (\Lambda_\alpha) \Big|_e = \left(\frac{A_x(\kappa_\alpha)x}{\Delta x} \right)_e \quad \alpha = r \text{ or } f \tag{17}$$

and

$$(\Psi_z) \Big|_a = \left(\frac{A_z \rho_f h g k_z}{\mu \Delta z} \right)_a, \quad (\Psi_z) \Big|_b = \left(\frac{A_z \rho_f h g k_z}{\mu \Delta z} \right)_b. \tag{18}$$

3.2 Linearization and operator splitting

Eqs. (11), (14) and (15) form a system of non-linear algebraic equations which must be solved numerically. The numerical solution strategy for the single-phase non-isothermal flow considered here predicts the calculation of each equation separately, applying an operator splitting (Dyrdaahl 2014) and a Picard linearization procedure (Nick *et al.* 2013).

When the calculation starts, for each time step, the values of p , T_f and T_r are estimated for an iterative level v and time $n + 1$. Then, fluid and rock properties are determined. Next, the pressure is calculated from the knowing values $T_f^{n+1,v}$ and $T_r^{n+1,v}$ obtained in the previous iteration. After that, the fluid temperature equation is solved using the new $p^{n+1,v+1}$ and old $T_r^{n+1,v}$ (not yet updated) values. Finally, the rock temperature is updated by solving the corresponding equation using $p^{n+1,v+1}$ and $T_r^{n+1,v+1}$ values recently calculated. Before a new iteration, all physical properties are updated from the new values of p , T_f and T_r .

The main advantage of the splitting method is the reduction of the number of calculations required for each time step. For instance, if there are N finite volumes, and we want to solve the coupled

system using a fully implicit scheme, we must solve $9N^2$ equations. On the other hand, for the uncoupled system, it can be reduced to $3N^2$ algebraic equations. However, it still will demand a lot of computer memory, and the computation time might be excessive (Vennemo 2016). Maes *et al.* (2016) investigated the application of operator splitting methods to the numerical modeling of in-situ upgrading of heavy oil, where heat is applied to the reservoir to decompose the heavier oil components into lighter, more mobile and more valuable liquid and gas components. They concluded in this study that operator splitting methods reduce computational effort when used to solve linear systems.

Nevertheless, as point out by Maes *et al.* (2016), a sequential implicit method introduces an additional error when we decouple the equations. As a result of this fact, we must use small time steps so that we can obtain the same accuracy of the fully coupled methods, and additional work would be necessary if we want to compare the computational times of the two approaches.

Hence, we are concerned with the numerical solution of three subsystems of linear algebraic equations, one for the pressure and two for the temperatures (oil and rock). Thus, for the pressure equation we have

$$\begin{aligned}
& \Phi_x \Big|_{i-1/2,j,k}^{n+1,v} p_{i-1,j,k}^{n+1,v+1} + \Phi_y \Big|_{i,j-1/2,k}^{n+1,v} p_{i,j-1,k}^{n+1,v+1} + \Phi_z \Big|_{i,j,k-1/2}^{n+1,v} p_{i,j,k-1}^{n+1,v+1} \\
& + \Phi_x \Big|_{i+1/2,j,k}^{n+1,v} p_{i+1,j,k}^{n+1,v+1} + \Phi_y \Big|_{i,j+1/2,k}^{n+1,v} p_{i,j+1,k}^{n+1,v+1} + \Phi_z \Big|_{i,j,k+1/2}^{n+1,v} p_{i,j,k+1}^{n+1,v+1} \\
& - \left[\overline{\Phi}_{x,y,z}^{n+1,v} + \frac{(\Gamma_p)_{i,j,k}^{n+1,v}}{\Delta t} \right] p_{i,j,k}^{n+1,v+1} = \frac{(\Gamma_p)_{i,j,k}^{n+1,v}}{\Delta t} p_{i,j,k}^n \\
& + \frac{(\Gamma_{T_f})_{i,j,k}^{n+1,v}}{\Delta t} \left[(T_f)_{i,j,k}^{n+1,v} - (T_f)_{i,j,k}^n \right] + \frac{(\Gamma_{T_r})_{i,j,k}^{n+1,v}}{\Delta t} \left[(T_r)_{i,j,k}^{n+1,v} - (T_r)_{i,j,k}^n \right] \\
& - (\Omega_z)_{i,j,k+1/2}^{n+1,v} (D_{i,j,k+1} - D_{i,j,k}) + (\Omega_z)_{i,j,k-1/2}^{n+1,v} (D_{i,j,k} - D_{i,j,k-1}) - q_{sc,i,j,k}^{n+1} \quad (19)
\end{aligned}$$

where

$$\overline{\Phi}_{x,y,z}^{n+1,v} = \Phi_x \Big|_{i+1/2,j,k}^{n+1,v} + \Phi_x \Big|_{i-1/2,j,k}^{n+1,v} + \Phi_x \Big|_{i,j+1/2,k}^{n+1,v} + \Phi_x \Big|_{i,j-1/2,k}^{n+1,v} + \Phi_x \Big|_{i,j,k+1/2}^{n+1,v} + \Phi_x \Big|_{i,j,k-1/2}^{n+1,v}. \quad (20)$$

For the temperature of the fluid, the following equation is considered

$$\begin{aligned}
& (\Lambda_f)_x \Big|_{i-1/2,j,k} T_{f,i-1,j,k}^{n+1,v+1} + (\Lambda_f)_y \Big|_{i,j-1/2,k} T_{f,i,j-1,k}^{n+1,v+1} + (\Lambda_f)_z \Big|_{i,j,k-1/2} T_{f,i,j,k-1}^{n+1,v+1} \\
& + (\Lambda_f)_x \Big|_{i+1/2,j,k} T_{f,i+1,j,k}^{n+1,v+1} + (\Lambda_f)_y \Big|_{i,j+1/2,k} T_{f,i,j+1,k}^{n+1,v+1} + (\Lambda_f)_z \Big|_{i,j,k+1/2} T_{f,i,j,k+1}^{n+1,v+1}
\end{aligned}$$

$$\begin{aligned}
 & - \left[(\bar{\Lambda}_f)_{x,y,z} + V_b AH + V_b \left(\frac{\rho C_{cp}}{\Delta t} \right)_{i,j,k}^{n+1,v} \right] T_{f,i,j,k}^{n+1,v+1} = -V_b \left(\frac{\rho C_{cp}}{\Delta t} \right)_{i,j,k}^{n+1,v} T_{f,i,j,k}^n \\
 & + (\Psi_z)_{i,j,k+1/2}^{n+1,v} (D_{i,j,k+1} - D_{i,j,k}) - (\Psi_z)_{i,j,k-1/2}^{n+1,v} (D_{i,j,k} - D_{i,j,k+1}) \\
 & + \bar{\Theta}_{x,y,z}^{n+1,v} - (\rho_f h q_{sc})_{i,j,k}^{n+1} - V_b AHT_{r,i,j,k}^{n+1,v} - \phi q_H \Big|_{i,j,k}^{n+1}. \tag{21}
 \end{aligned}$$

where

$$\begin{aligned}
 \frac{\bar{\Theta}_{x,y,z}^{n+1,v}}{\rho_{fsc}} & = (h\Phi_x)_{i-1/2,j,k}^{n+1,v} (p_{i,j,k} - p_{i-1,j,k})^{n+1,v+1} - (h\Phi_x)_{i+1/2,j,k}^{n+1,v} (p_{i+1,j,k} - p_{i,j,k})^{n+1,v+1} \\
 & + (h\Phi_y)_{i,j-1/2,k}^{n+1,v} (p_{i,j,k} - p_{i,j-1,k})^{n+1,v+1} - (h\Phi_y)_{i,j+1/2,k}^{n+1,v} (p_{i,j+1,k} - p_{i,j,k})^{n+1,v+1} \\
 & + (h\Phi_z)_{i,j,k-1/2}^{n+1,v} (p_{i,j,k} - p_{i,j,k-1})^{n+1,v+1} - (h\Phi_z)_{i,j,k+1/2}^{n+1,v} (p_{i,j,k+1} - p_{i,j,k})^{n+1,v+1} \tag{22}
 \end{aligned}$$

and

$$\begin{aligned}
 (\bar{\Lambda}_f)_{x,y,z} & = (\Lambda_f)_x \Big|_{i,j+1/2,k} + (\Lambda_f)_x \Big|_{i-1/2,j,k} + (\Lambda_f)_y \Big|_{i,j+1/2,k} \\
 & + (\Lambda_f)_y \Big|_{i,j-1/2,k} + (\Lambda_f)_z \Big|_{i,j,k+1/2} + (\Lambda_f)_z \Big|_{i,j,k-1/2}. \tag{23}
 \end{aligned}$$

Finally, for the rock temperature,

$$\begin{aligned}
 & (\Lambda_r)_x \Big|_{i-1/2,j,k} T_{r,i-1,j,k}^{n+1,v+1} + (\Lambda_r)_y \Big|_{i,j-1/2,k} T_{r,i,j-1,k}^{n+1,v+1} + (\Lambda_r)_z \Big|_{i,j,k-1/2} T_{r,i,j,k-1}^{n+1,v+1} \\
 & + (\Lambda_r)_x \Big|_{i+1/2,j,k}^{n+1} T_{r,i+1,j,k}^{n+1,v+1} + (\Lambda_r)_y \Big|_{i,j+1/2,k} T_{r,i,j+1,k}^{n+1,v+1} + (\Lambda_r)_z \Big|_{i,j,k+1/2} T_{r,i,j,k+1}^{n+1,v+1} \\
 & - \left\{ (\bar{\Lambda}_r)_{x,y,z} + V_b AH + V_b \left[\frac{(1-\phi)\rho C_{cp}}{\Delta t} \right]_{i,j,k}^{n+1,v} \right\} T_{r,i,j,k}^{n+1,v+1} = -V_b AHT_{f,i,j,k}^{n+1,v+1} \\
 & - V_b \left[\frac{(1-\phi)\rho_r C_{cp}}{\Delta t} \right]_{i,j,k}^{n+1,v} T_{r,i,j,k}^n - (1-\phi)q_H \Big|_{i,j,k} \tag{24}
 \end{aligned}$$

where,

$$(\bar{\Lambda}_r)_{x,y,z} = (\Lambda_r)_x \Big|_{i,j+1/2,k}^{n+1} + (\Lambda_r)_x \Big|_{i-1/2,j,k}^{n+1} + (\Lambda_r)_y \Big|_{i,j+1/2,k}^{n+1}$$

$$+ (\Lambda_r)_y \Big|_{i,j-1/2,k}^{n+1} + (\Lambda_r)_z \Big|_{i,j,k+1/2}^{n+1} + (\Lambda_r)_z \Big|_{i,j,k-1/2}^{n+1}. \tag{25}$$

3.3 Numerical solution of the linear subsystems

The third step of the FVM consists of the solution of the set of algebraic equations, Eqs. (19), (21) and (24). Here we chose the Conjugate Gradient Method, a well known and efficient iterative algorithm, to solve the three subsystems of linear equations (Ertekin, Abou-Kassem and King 2001), knowing that the coefficient matrices are symmetric.

Fig. 3 depicts the main steps performed by the numerical code to obtain the values of p , T_f and T_r using the linearization, the operator splitting, and the Conjugate Gradient Method (CG).

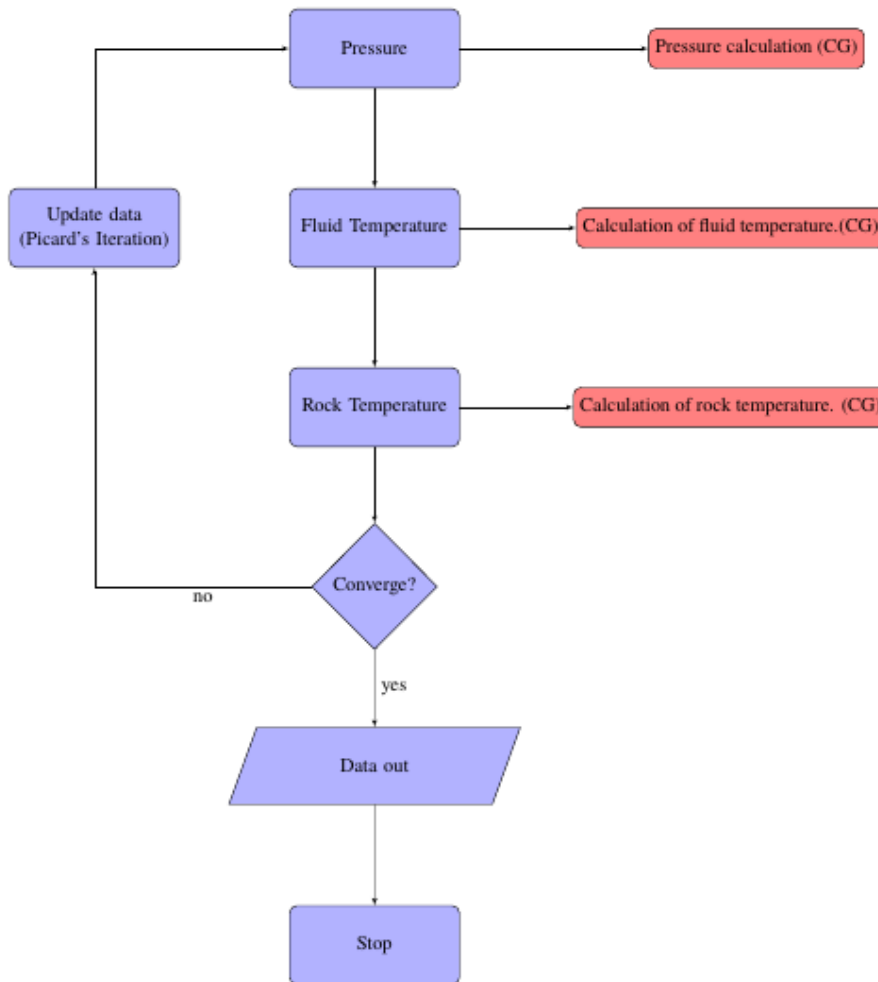


Fig. 3 Flowchart of the numerical solution of the subsystems

4. Results and discussions

This section is dedicated to present and discuss the numerical results. The first subsection introduces our default case. The following three subsections contain a sensibility analysis considering the influence of the heaters and different values for heat transfer coefficient and porosity. The last subsection is devoted to the comparison between the one- and two-equation models.

4.1 Default case

All pressure and temperature fields are obtained having as start point our default case. So we have a vertical production well positioned in the middle of the xy -plan of the reservoir, and oil is produced at a prescribed flow rate given by $Q_{sc} = \sum_1^{n_z} q_{sc}$ (n_z is the cell numbers in z direction). The static heaters are placed around the production well in a specific arrangement. We decided to place four heaters (two in the x -direction and two in the y -direction, all parallel to z - direction) whose distance to the producing well is equal to L_T . In Tab. 1 we find the properties (porosity and permeability), distance from each heater to the well, the lengths (L_x , L_y and L_z) of the reservoir, the flow rate, the electric power of the heaters ($Q_H = \sum_1^{n_z} q_H$), and the effective heat transfer coefficient.

Table 1 Properties of the reservoir

Parameter	Unit	Value	Parameter	Unit	Value
$\phi_{init} = \phi^0$	-	0.3	L_z	m	120
$k_x = k_y = k_z$	m ²	$1.0 \cdot 10^{-15}$	Q_{sc}	STB/day	-10.0
L_T	m	40	Q_H	kW	320
$L_x = L_y$	m	$1.840 \cdot 10^3$	H	W/m ² K	2,000

Other important parameters are given in Table 2: initial time step (Δt_{init}), final time step (Δt_{max}), time step increase rate ($F_{\Delta t}$), maximum simulation time (t_{max}), initial pressure (P_{init}), initial temperatures for fluid ($T_{f_{ini}}$) and rock ($T_{r_{ini}}$), and the number of cells (n_x , n_y and n_z) in the three spatial directions.

Table 2 Parameters for the numerical simulation

Parameter	Unit	Value	Parameter	Unit	Value
Δt_{init}	day	$1.0 \cdot 10^{-1}$	$T_{r_{ini}}$	K	330
Δt_{max}	day	1.0	$T_{f_{ini}}$	K	330
$F_{\Delta t}$	-	1.1	n_x	-	185
t_{max}	day	200	n_y	-	185
P_{init}	kPa	$1.0 \cdot 10^4$	n_z	-	5

Table 3 presents the properties with respect to the fluid (oil): standard and reference pressures, standard temperature, reference temperature to determine the fluid viscosity, density and formation-volume-factor of reference, a and b parameters for Eq. (3), coefficient of compressibility, coefficient

of thermal expansion, heat capacity, and thermal conductivity.

Table 3 Fluid Properties

Parameter	Unit	Value	Parameter	Unit	Value
p_{sc}	kPa	101.3	a	Pa.s	$8.0 \cdot 10^{-4}$
p^0	kPa	$69 \cdot 10^3$	b	K	333.33
T_{sc}	K	277.78	c_f	kPa^{-1}	$7.25 \cdot 10^{-7}$
$T_{ref\mu}$	K	277.7	c_{fT}	K^{-1}	$9.2 \cdot 10^{-4}$
ρ^0	kg/m^3	1,034	c_{pf}	J/kg.K^3	2,100
B^0	RB/STB	1.3	κ_f	W/m K	0.1225

Lastly, the properties of the rock are shown in Table 4: density, superficial specific area of the fluid-rock interface, heat capacity, coefficient of compressibility, coefficient of thermal expansion, and thermal conductivity.

Table 4 Rock properties

Parameter	Unit	Value	Parameter	Unit	Value
ρ_r	kg/m^3	2,500	c_r	kPa^{-1}	$4.35 \cdot 10^{-7}$
A	m^{-1}	200	c_{rT}	K^{-1}	$1.8 \cdot 10^{-3}$
c_{pr}	J/kg.K	1,200	κ_r	W/m K	4.5

The mesh we used in all simulations was chosen after a numerical convergence study, considering the same flow and physical properties of the default case, but without heater-wells (see Fig. 4).

4.2 Static heaters

Our main goal is the study of the effect of static heating on heavy oil recovery. Hence, we compare pressure and temperature curves calculated with and without heating considering that $H=2,000 \text{ W/m}^2\text{K}$.

In Fig. 5, we can see the pressure distribution along the x -axis. There is a significant reduction of the pressure gradient, near the producing well, when we use static heaters. It is mainly due to oil viscosity reduction, which reduces the resistance to flow according to Darcy's law. Therefore, a lower pressure gradient is required to produce the same amount of oil (remind that the flow rate is kept fixed).

Fluid and rock temperatures (Figs. 6 and 7) increase near the heaters as consequence of the extra energy supply by them. We can also observe a temperature reduction for both fluid and rock where the producing well is positioned due to the energy being withdrawn from the reservoir at that region.

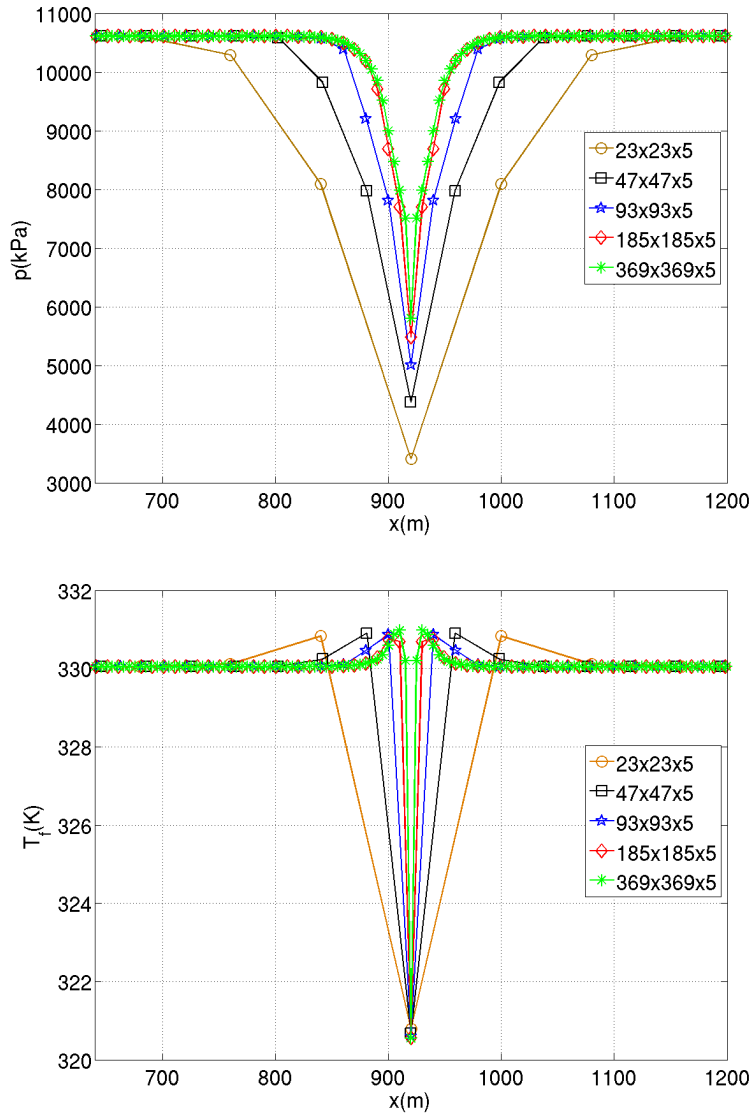
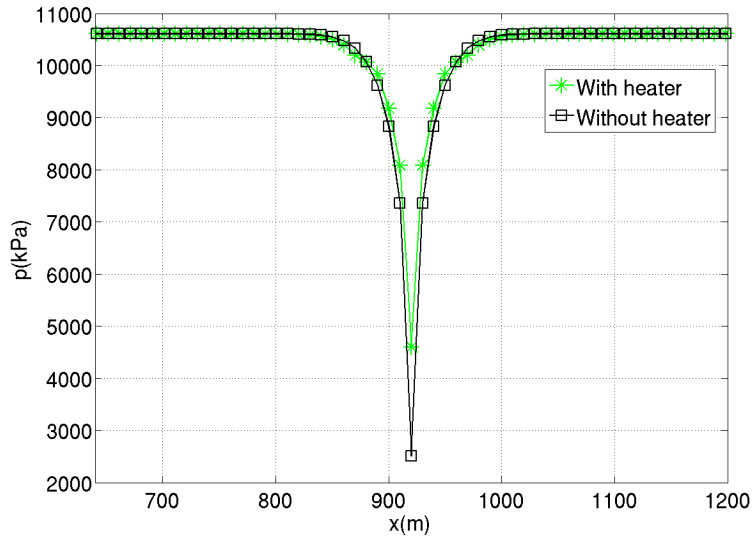
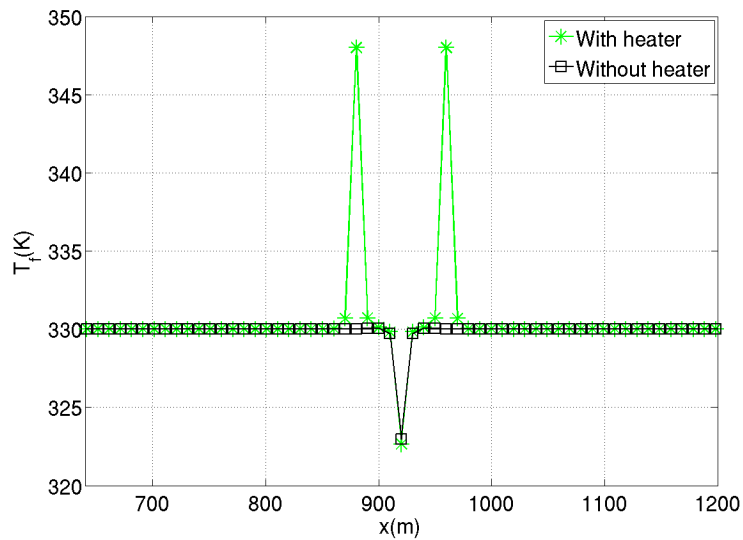


Fig. 4 Numerical convergence study for different $n_x \times n_y \times n_z$ meshes

4.3 Heat transfer coefficient

We now investigate the influence of the coefficient of heat transfer H . This parameter appears explicitly in the source terms in the macroscopic energy equations for both fluid and rock phases, and it takes into account the macroscopic heat exchanged between the fluid and the rock when there is a temperature gradient. This coefficient is usually estimated experimentally, and its determination is a difficult task when describing the heat transfer process (Lampe 2013). Typical values of this coefficient range from 100-20,000 $\text{W/m}^2\text{K}$ and according to Lampe (2013) it may be defined as a

Fig. 5 Pressure in the reservoir for $H=2,000 \text{ W/m}^2\text{K}$ Fig. 6 Fluid temperature for $H=2,000 \text{ W/m}^2\text{K}$

harmonic average of thermal conductivities.

Another possible approach to calculate this coefficient uses the Nusselt number to approximate the H value. Hsieh and Lu (2000) consider that the Reynolds number plays a key role and as a consequence velocity and viscosity are important parameters to determine H . Therefore, when the

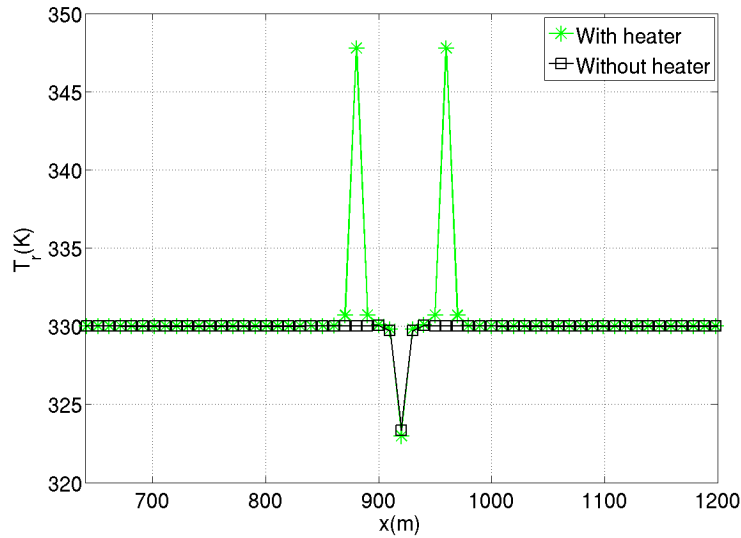


Fig. 7 Rock temperature for $H=2,000 \text{ W/m}^2\text{K}$

fluid velocity is low (or the viscosity is high), the H value tends to be low. The opposite applies when the fluid velocity is high, or the viscosity is low. However, in the present work, we only consider a range of values to verify the effect that the coefficient has on the temperature and pressure distributions.

In Fig. 8, we represent $|T_f - T_r|$ as a function of the position x for four different values of H : 200, 400, 800 and $1,600 \text{ W/m}^2\text{K}$. We note that the higher the coefficient value, the smaller the temperature difference between the fluid and rock. As the H coefficient increases, more energy is transferred between the phases, and the phases will tend to the local thermal equilibrium. Otherwise, when the coefficient of heat transfer decreases each phase will store more energy and the temperature difference will be higher.

Furthermore, the temperature difference is greater near the heaters and producing well, where there are an energy source and a heat sink. As the thermal properties of the fluid and rock are different so are the temperatures, since, near the heaters (energy sources) accumulation, advection (only for oil) and heat conduction are different depending on the phase considered. On the other hand, on the producing well more energy is being withdrawn from the fluid as it is produced.

4.4 Porosity

Next, the objective is to evaluate the influence of porosity on pressure and temperature. In Fig. 9 we can verify that the pressure gradient increases when porosity decreases, with respect to the reservoir pressure far away from the producing well. For the three values, the lower the porosity, the lower is the pressure at the producing well. If we want to recover the same amount of oil, for a fixed flow rate, it is necessary a greater pressure gradient for a lower porosity.

With regard to temperatures, Fig. 10 shows the fluid temperature as a function of the porosity

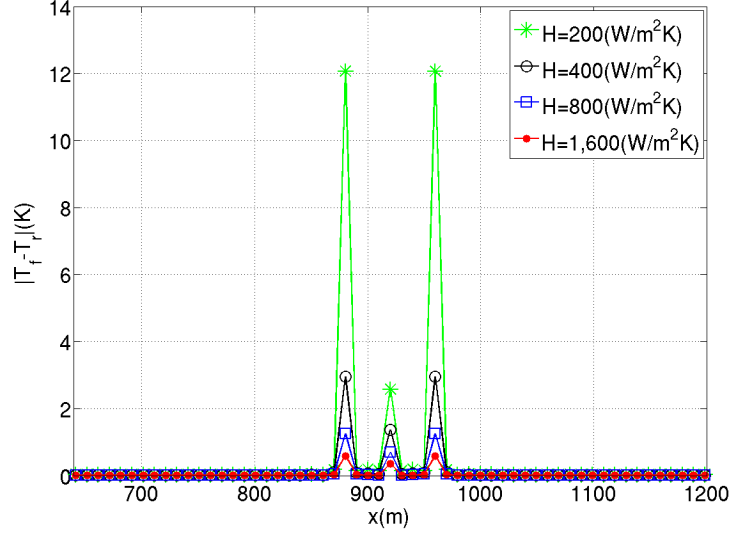


Fig. 8 Temperature difference $|T_f - T_r|$ for $H=200, 400, 800$ and $1,600 \text{ W/m}^2\text{K}$

($\phi=0.2, 0.3$ and 0.4). In the regions near the heaters the higher is the porosity, the higher is the fluid temperature. This happens because the fluid heat capacity is high and, therefore, its capacity to store energy and vice-versa. The rock temperature presents the same fluid temperature pattern as we can see in Fig. 11. We can explain this behavior by considering that the heat transfer coefficient is relatively high, $H=2,000 \text{ W/m}^2\text{K}$, and there is an important transfer of energy between both phases (fluid and rock) leading to a thermal equilibrium.

4.5 Thermal equilibrium hypothesis

In general, we can use a one- or two-equation models to simulate heat transfer in porous media. For the one-equation model we can assume ($T_f = T_r$) (Rousset, Huang and Durlofsky 2014) or not ($T_f \neq T_r$) the hypothesis of local thermal equilibrium (Moyne *et al.* 2000). Although simpler, the one-equation model is not suitable to be applied to all heat transfer problems, depending on the order of magnitude of the thermal properties of the fluid and rock (Moyne and Amaral Souto 2014a, b). In this work, to investigate the feasibility of the use of the two models, simulations were performed employing both models: a one-equation model as proposed by Moyne *et al.* (2000) and a two-equation model (similar to that used by Lampe (2013)).

In the two-equation model, as already stated, there are two macroscopic energy equations, one for each phase (fluid and rock). On the other hand, the one-equation model considered here introduces an average temperature (for the reservoir) that is obtained from the fluid and rock temperatures (Moyne *et al.* 2000)

$$\overline{\rho c_p} T = \phi \rho_f c_{p_f} T_f + (1 - \phi) \rho_r c_{p_r} T_r \quad (26)$$

where $\overline{\rho c_p} = \phi \rho_f c_{p_f} + (1 - \phi) \rho_r c_{p_r}$ is the average heat capacity of the reservoir.

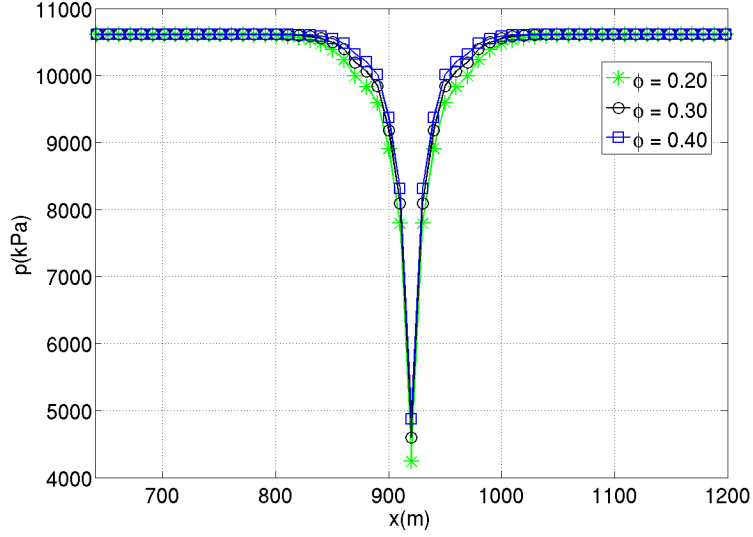


Fig. 9 Pressure in the reservoir for $\phi=0.2, 0.3$ and 0.4

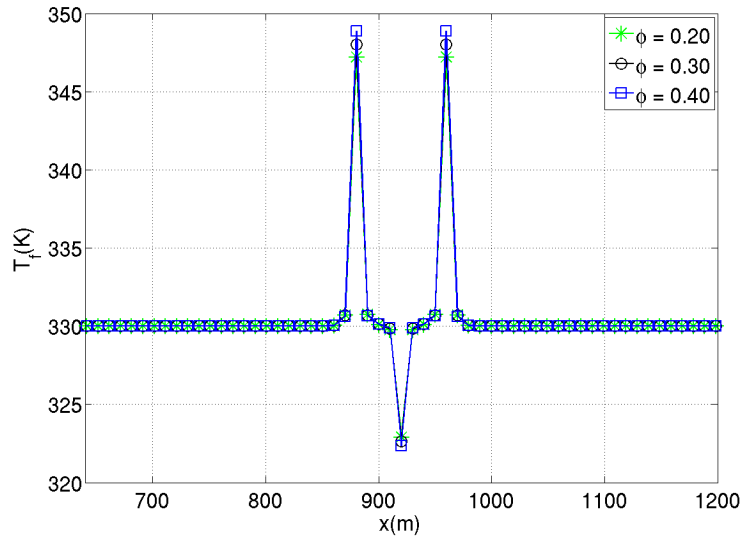


Fig. 10 Fluid temperature for $\phi=0.2, 0.3$ and 0.4

The energy governing equation for this model is given by (Moyne *et al.* 2000)

$$\frac{\partial}{\partial t}(\overline{\rho c_p} T) + \nabla \cdot (\rho_f h_f \mathbf{v}) - \nabla \cdot (\mathbf{K} \nabla T) - \frac{q_H}{V_b} - \frac{\rho_f h_f q_{sc}}{V_b} = 0. \quad (27)$$

Without considering neither tortuosity nor hydrodynamic dispersion, the thermal dispersion tensor is

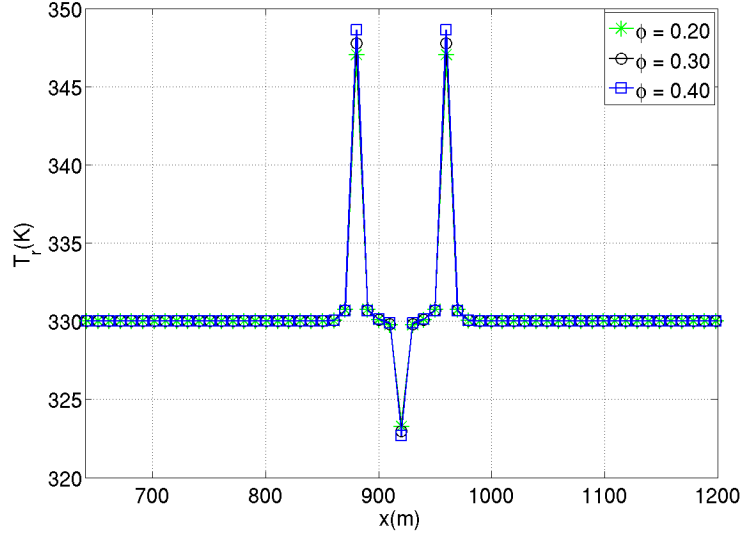


Fig. 11 Rock temperature for $\phi=0.2, 0.3$ and 0.4

reduced to

$$\mathbf{K} = [\phi\kappa_f + (1 - \phi)\kappa_r] \mathbf{I}. \quad (28)$$

As there is a source term in the two-equation model, in both equations, that depends on the specific area A , the heat transfer coefficient H , and the temperature difference between the fluid and rock, a set of tests was carried out to determine the influence of the heat transfer coefficient. As we know, this source term is responsible for estimating the energy transfer from the fluid to the rock and vice-versa.

Now, to compare the temperatures of the reservoir issue from the two-models, a new average temperature (T_2) is calculate according to Eq. (26) using T_r and T_f values determined with Eqs. (9) and (10) respectively. Thus, Figs. 12, 13, 14 and 15 contain the temperature distribution along the x -axis for T_r , T_f , $T_1 = T$ (temperature of the reservoir determined with the one-equation model, Eq. (27)) and T_2 for four different H values.

We realize that for $H=200$ W/m²K (Fig. 12) the average temperatures T_1 and T_2 are different and the results do not match for the one- and two-equation models and $T_f \neq T_r$. As we increase the heat transfer coefficient, we observe that the temperature T_2 tends to converge to the values predicted by the one-equation model (T_1). For example, in Fig. 13 there is only a slight difference between the temperatures T_1 and T_2 , and still $T_f \neq T_r$. With $H=800$ and $1,600$ W/m²K, Figs 14 and 15, we can consider that the system has attained the local thermal equilibrium and $T_f = T_r = T_1 = T_2$, Fig. 15. However, the one-equation model does not directly provide fluid and rock temperatures when they are different, but rather the average reservoir temperature.

We emphasize that these conclusions apply only to the variation of the heat transfer coefficient (see Lampe (2013) for the range of H). However, properties such as the relationship between thermal diffusivity and thermal conductivity play a fundamental role in the accuracy of the two models (Moyné

and Amaral Souto 2014a, b).

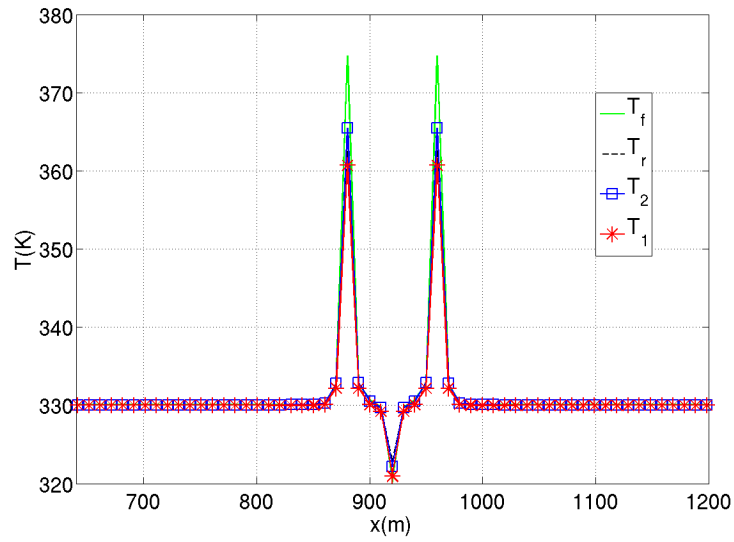


Fig. 12 Temperature distribution in the reservoir considering $H=200 \text{ W/m}^2\text{K}$

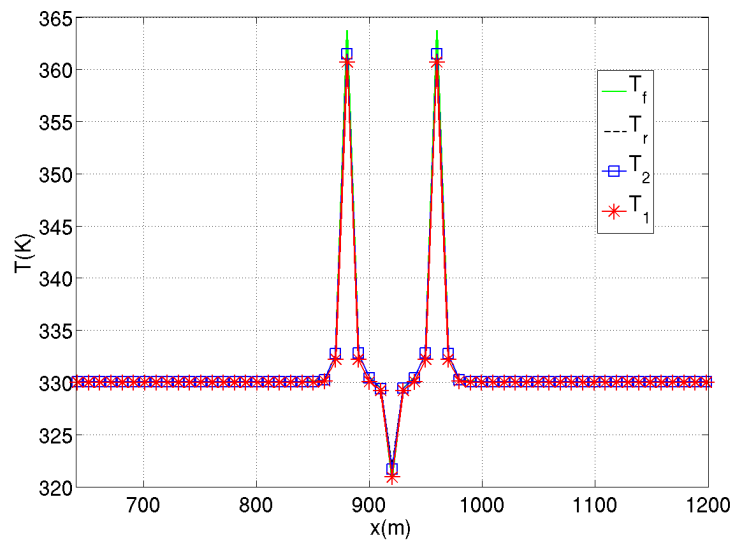


Fig. 13 Temperature distribution in the reservoir considering $H=400 \text{ W/m}^2\text{K}$

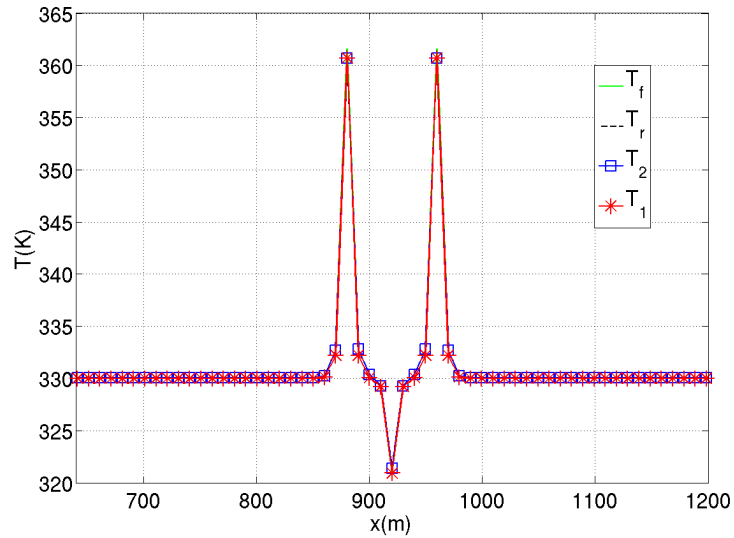


Fig. 14 Temperature distribution in the reservoir considering $H=800 \text{ W/m}^2\text{K}$

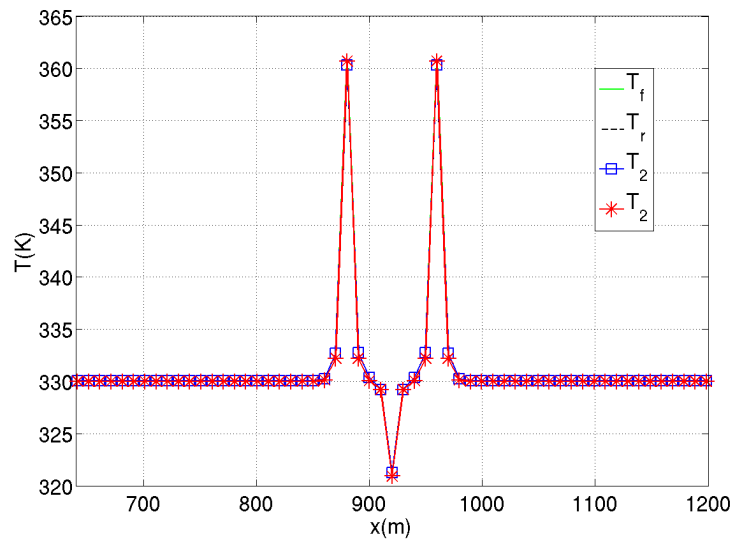


Fig. 15 Temperature distribution in the reservoir considering $H=1,600 \text{ W/m}^2\text{K}$

5. Conclusions

In this work, we investigated an enhanced oil recovery thermal method, and a set of tests were performed to verify the feasibility of this recovery method using static heaters.

The sensibility analysis shows that significant gain can be achieved in oil recovery using static

heaters, due to the decrease in heavy oil viscosity as well as of the resistance to flow through the reservoir. Therefore, for a fixed flow rate, the same amount of oil can be produced with a lower pressure gradient as a result of this reduction.

The heat transfer coefficient, besides the thermal properties, has an important role since for higher H values both one- and two-equation models tend to provide the same results for the reservoir temperature. Moreover, in these cases, even the local thermal equilibrium can be attained and the equality between fluid and rock temperatures can be a good approximation. Otherwise, for lower values the two-equation model is best suited to be used in practice. In this work the determination of this coefficient was not studied in depth, but for future works it will be investigated.

Acknowledgements

Authors gratefully thanks Rio de Janeiro State University, Coordination for the Improvement of Higher Education Personnel (CAPES) - Finance Code 001, National Council for Scientific and Technological Development (CNPq) and Rio de Janeiro Research Foundation (FAPERJ) for their support.

References

- Aouizerate, G., Durlofsky, L.J. and Samier, P. (2011), "New models for heater wells in subsurface simulations, with application to the in situ upgrading of oil shale", *Comput. Geosci.*, **16**(2), 519-533.
- Dyrdahl, J. (2014), "Thermal flow in fractured porous media and operator splitting", M.Sc. Dissertation, Norwegian University of Science and Technology, Norway.
- Eduardo, R. (2010), "A comprehensive model describing temperature behavior in horizontal wells: Investigation of potential benefits of using downhole distributed temperature measurement system", Ph.D. Dissertation, The Pennsylvania State University, U.S.A.
- Ertekin, T., Abou-Kassem, J. and King, G. (2001), *Basic Applied Reservoir Simulation*, Richardson, Society of Petroleum Engineers, U.S.A.
- Ezeuko, C.C. and Gates, I.D. (2018), "Thermal oil recovery from fractured reservoirs: Energy and emissions intensities", *Energy*, **155**, 29-34.
- Hazra, K.G. (2014), "Comparison of heating methods for in-situ oil shale extraction", Ph.D. Dissertation, Texas AM University, Texas, U.S.A.
- Hadzalic, E., Ibrahimbegovic, A. and Dolarevic, S. (2018), "Failure mechanisms in coupled soil-foundation systems", *Coupled Syst. Mech.*, **7**(1), 27-42.
- Hadzalic, E., Ibrahimbegovic, A. and Nikolic, M. (2018), "Failure mechanisms in coupled poro-plastic medium", *Coupled Syst. Mech.*, **7**(1), 43-59.
- Hsieh, W.H. and Lu, S.F. (2000), "Heat-transfer analysis and thermal dispersion in thermally-developing region of a sintered porous metal channel", *Int. J. Heat Mass Transf.*, **43**(16), 3001-3011.
- Lampe, V. (2013), "Modelling fluid flow and heat transport in fractured porous media", M.Sc. Dissertation, University of Bergen, Norway.
- Maes, J., Muggeridge, A.H., Jackson, M.D., Quintard, M. and Lapene, A. (2016), "Modelling in-situ upgrading of heavy oil using operator splitting method", *Comput. Geosci.*, **20**(3), 581-594.
- Manichand, R.N. (2002), "Análise do desempenho do aquecimento eletromagnético na recuperação de reservatórios de petróleo", M.Sc. Dissertation, Rio Grande do Norte State University, Rio Grande do Norte,

Brazil.

- Moyne, C. and Amaral Souto, H.P. (2014), “Multi-scale approach for conduction heat transfer: One-and two-equation models. Part 1: Theory”, *Comput. Appl. Math.*, **33**(1), 257-274.
- Moyne, C. and Amaral Souto, H.P. (2014), “Multi-Scale approach for conduction heat transfer: One and two-equation models. Part 2: Results for a stratified medium”, *Comput. Appl. Math.*, **33**(2), 433-449.
- Moyne, C., Didierjean, S., Amaral Souto, H.P. and Da Silveira, O.T. (2000), “Thermal dispersion in porous media: one-equation model”, *Int. J. Heat Mass Transf.*, **43**(20), 3853-3867.
- Moukalled, F., Mangani, L. and Darwish, M. (2016), *The Finite Volume Method in Computational Fluid Dynamics: An Advanced Introduction with OpenFOAM and Matlab*, Springer, Fluid Mechanics and Its Applications, Switzerland.
- Nick, H.M., Raouf, A., Centler, F., Thullner, M. and Regnier, P. (2013), “Reactive dispersive contaminant transport in coastal aquifers: Numerical simulation of a reactive Henry problem”, *J. Contamin. Hydrol.*, **145**, 90-104.
- Nikolic, M., Ibrahimbegovic, A. and Miscevic, P. (2016), “Discrete element model for the analysis of fluid-saturated fractured poro-plastic medium based on sharp crack representation with embedded strong discontinuities”, *Comput. Meth. Appl. Mech. Eng.*, **298**, 407-427.
- Rousset, M.A.H., Huang, C.K. and Durlofsky, H.K.J. (2014), “Reduced-order modeling for thermal recovery processes”, *Comput. Geosci.*, **18**(3-4), 401-415.
- Vennemo, S.B. (2016), “Multiscale simulation of thermal flow in porous media”, M.Sc. Dissertation, Norwegian University of Science and Technology, Trondheim, Norway.

AI